Brazilian Journal of Geophysics (2021) 39(1): 71–83
© 2021 Sociedade Brasileira de Geofísica
ISSN 0102-261X
www.rbgf.org.br
DOI: 10.22564/rbgf.v38i3.2061

THE GENERALIZED CROSS VALIDATION METHOD FOR THE SELECTION OF THE REGULARIZATION PARAMETER IN GEOPHYSICAL DIFFRACTION TOMOGRAPHY

Eduardo T. F. Santos [1], Amin Bassrei [2*] and Jerry M. Harris [3*]

ABSTRACT. Inverse problems are usually ill-posed in such a way that it is necessary to use some method to reduce their deficiencies. For this purpose, we use the regularization by derivative matrices, known as Tikhonov regularization. There is a crucial problem in regularization, which is the selection of the regularization parameter λ. In this work, we use generalized cross validation (GCV) as a tool for the selection of λ. GCV is used here for an application in geophysical diffraction tomography, where the objective is to obtain the 2-D velocity distribution from the measured values of the scattered acoustic field. The results are compared to those obtained using L-curve, and also Θ-curve, which is an extension of L-curve. We present several simulation results with synthetic data, and in general the results using GCV are equal or eventually better than the other two approaches.

Keywords: seismic inversion, tomography, reservoir characterization.

RESUMO. Os problemas inversos são geralmente mal postos de tal forma que é necessário usar algum método para reduzir suas deficiências. Para este propósito, utilizamos a regularização por matrizes derivadas, conhecida como regularização de Tikhonov. Há um problema crucial no procedimento da regularização, que é a seleção do parâmetro de regularização λ. Neste trabalho, usamos a validação cruzada generalizada (GCV) como uma ferramenta para a seleção do λ. O GCV é usado aqui para uma aplicação em tomografia geofísica de difração, em que o objetivo é obter a distribuição 2-D da velocidade a partir dos valores medidos do campo acústico espalhado. Os resultados são comparados aos obtidos usando a curva L, e também a curva Θ, que é uma extensão da curva L. Apresentamos vários resultados de simulação com dados sintéticos e, em geral, os resultados usando GCV são iguais ou eventualmente melhores do que as outras duas abordagens.

Palavras-chave: inversão geofísica, tomografia sísmica, caracterização de reservatórios.

Corresponding author: Amin Bassrei

[1]Instituto Federal da Bahia - IFBA, Rua Emídio dos Santos, S/N Barbalho, 40300-010 Salvador, BA, Brazil – E-mail: eduardot@ifba.edu.br

[2]Universidade Federal da Bahia - UFBA, Instituto de Geociências, Centro de Pesquisa em Geofísica e Geologia (CPGG/IGEO), and Instituto Nacional de Ciência e Tecnologia de Geofísica do Petróleo (INCT/GP), Rua Barão de Jeremoabo, s/n, Campus Universitário de Ondina 40170-115 Salvador, BA, Brazil, Phone: +(55)(71)3283-8508 – E-mail: bassrei@ufba.br

[3]Stanford University, Department of Geophysics, Stanford, CA, USA – E-mail: jerry.harris@stanford.edu

INTRODUCTION

The petroleum industry is the major user of geophysical inverse methods for subsurface imaging. Among the different methods, seismic methods (or exploration seismology methods) are the most common. There are two main classes of seismic tomography or more correctly acoustical tomography: those that use only kinematic traveltimes between sources and receivers, and those that use the wave amplitudes, i.e., a dynamic approach. In this work, we use a special kind of the latter, known in the literature as geophysical diffraction tomography (GDT). In GDT, the input data is the scattered acoustic field measured at the receivers, and the velocity of the medium is the inversion output. Instead of using the classical approach of GDT, that is, Fourier projection theorem (Devaney, 1984; Slaney et al., 1984; Harris, 1987; Wu & Toksöz, 1987), we use a matrix formulation approach (Thompson et al., 1994; Reiter & Rodi, 1996; Rocha-Filho et al., 1996; Rocha-Filho et al., 1997). The main advantages of the matrix formulation are: (1) the option of having irregular spacing (i) between sources, (ii) between receivers and (iii) between sources and receivers (all very common in practical situations with real data); and (2) the possibility to study, in a better way, the ill-posedness of the inverse problem.

We use scattered acoustic data simulated with a 2-D finite difference scheme, e.g., second order in time and fourth order in space. The tomographic matrix is computed using a first order Born approximation. GDT is an ill-posed inverse problem, so it is necessary to use some tool to reduce this deficiency. The tool that we choose is the regularization of the inverse problem by derivative matrices, known in the literature by several names, in particular Tikhonov regularization. One regularization parameter, λ, whose choice is already a problem, plays an especially crucial role.

There are several techniques to find the optimum λ, for example, the L-curve. In geophysical applications that employed the L-curve, one could mention Santos and Bassrei (2007) in GDT, and Giraud et al. (2019) who used L-curve in joint inversion of petrophysical and geophysical data. In other areas outside geophysics, Niknam Shahrak et al. (2013) used, among different techniques, the L-curve as a method to choose λ in a pore size distribution determination problem. Recently, Guizar-Sicairos et al. (2020) used the L-curve in an X-ray scattering problem.

Besides using the L-curve, Santos & Bassrei (2007) proposed a variation of it, called the Θ-curve. The application of the Θ-curve as a method for the selection of optimum λ was employed in other application. For instance, Rodrigues & Bassrei (2016) used Θ-curve in traveltime tomography in real data from the Recôncavo Basin, state of Bahia, Brazil. And in correlated areas to GDT, one could mention the work of Zhang (2011), who used Θ-curve and a variation of it, called improved Θ-curve, in near field acoustic holography.

Yao & Roberts (1999) used the generalized cross-validation (GCV) for the choice of the regularization parameter in linear seismic tomographic inversion. The GCV technique suggests that a good value for the regularization parameter λ should predict which element of the data vector is missing or has been removed. More precisely, if an element of the data vector is removed, then the corresponding regularized solution must predict this absence well. GCV has been used in several papers related to geophysical applications. Mojica & Bassrei (2015) used GCV to select the optimum λ in the inversion of 3-D gravity data with parallel processing. Oliveira & Bassrei (2015) used GCV to select the optimum λ in electromagnetic tomography. In GDT, Silva & Bassrei (2016) used GCV to select the optimum λ in an application of multifrequency GDT as a tool for CO_2 monitoring and Sande et al. (2019) used GCV to select the optimum λ in an iterative

multifrequency GDT where the background medium is not assumed to be known. In other applications outside geophysics, one could mention Lay-Ekuakille et al. (2010) who used GCV in a problem of leak detection of pipelines. Farquharson & Oldenburg (2004) compared GCV and L-curve for geophysical applications in non-linear inversion of electromagnetic data.

This paper has the following structure: the theories of linear inversion and regularization are reviewed, and the GCV technique is presented; then we review the theory of diffraction tomography within the framework of the Born approximation. For the simulations, we use the GCV method in GDT for two acquisition geometries: cross-hole and vertical seismic profile (VSP). We compare the GCV results with two other approaches: L-curve and Θ-curve.

Linear Inversion, Regularization and Generalized Cross Validation

Consider a modeling process where the input to some system is described by parameters contained in $\mathbf{m}$ and the output is described as $\mathbf{Am}$ which is a linear transformation on $\mathbf{m}$. If the vector $\mathbf{d}$ describes the "observed" output of the system, the problem will be to "choose" the parameters $\mathbf{m}$ in order to minimize in some sense the difference between the observed $\mathbf{d}$ and the prescribed output of the system $\mathbf{Am}$. If we measure this difference through the norm $\|\bullet\|$, our task will be to find the value of $\mathbf{m}$ which minimizes

$$\|\mathrm{Am}-\mathrm{d}\|_2, \tag{1}$$

where the $M \times N$ matrix $\boldsymbol{A}$ and the data vector $\boldsymbol{d}$ with M elements are provided to the problem (Menke, 2012). This is called a least squares problem, which can be formally stated as follows. Considering the basic relationship

$$\mathrm{d}=\mathrm{Am}+\mathrm{e}, \tag{2}$$

we wish to minimize the error using the following objective function:

$$\Phi(\boldsymbol{m}) = \boldsymbol{e}^T\boldsymbol{e} + \lambda L_2, \tag{3}$$

where the error is given by $\mathbf{e} = \mathbf{d} - \mathbf{Am}$, λ is a scalar called the damping parameter, and $L_2 = \mathbf{m}^T\mathbf{m}$. The estimated solution of Equation (3), also called the damped least squares (DLS) solution, is

$$\mathbf{m}^{est} = (\mathbf{A}^T\mathbf{A} + \lambda\mathbf{I})^{-1}\mathbf{A}^T\mathbf{d}^{obs}. \tag{4}$$

The inverse of matrix $(\mathbf{A}^T\mathbf{A} + \lambda\mathbf{I})$ is usually calculated using the singular value decomposition (SVD). A rectangular $M \times N$ matrix $\boldsymbol{A}$ with rank k can be decomposed as $\mathbf{A} = \mathbf{U\Sigma}\ \ \mathbf{V}^T$, where $\mathbf{U}$ is the $M \times M$ matrix which contains the orthonormalized eigenvectors of $\mathbf{AA}^T$; $\boldsymbol{V}$ is the $N \times N$ matrix which contains the orthonormalized eigenvectors of $\mathbf{A}^T\mathbf{A}$; and $\mathbf{\Sigma}$ is the $M \times N$ matrix which contains the singular values of $\boldsymbol{A}$, written in decreasing order, that is, $\sigma_1 \geq \sigma_2 \geq \cdots \geq \sigma_k$. The GI $\mathbf{A}^+$ is a $N \times M$ matrix given by $\mathbf{A}^+ = \mathbf{V\Sigma}^+\mathbf{U}^T$, where $\mathbf{\Sigma}^+$ is the $N \times M$ matrix which contains the reciprocals of the non-zero singular values of $\mathbf{A}$, so that

$$\boldsymbol{\Sigma}^+ = \begin{pmatrix} \boldsymbol{E} & 0 & \cdots & 0 \\ 0 & 0 & \cdots & 0 \\ \cdots & \cdots & \ddots & \vdots \\ 0 & 0 & \cdots & 0 \end{pmatrix}, \tag{5}$$

and $\boldsymbol{E}$ is the diagonal square matrix of order k expressed by

$$\boldsymbol{E} = \begin{pmatrix} \sigma_1^{-1} & 0 & \cdots & 0 \\ 0 & \sigma_2^{-1} & \cdots & 0 \\ \cdots & \cdots & \ddots & \vdots \\ 0 & 0 & \cdots & \sigma_k^{-1} \end{pmatrix}. \tag{6}$$

Least-squares solutions very often do not provide good results and sometimes they do not even exist. In order to solve this problem, we use the tool of regularization or smoothing: the ill-conditioning of the matrix $\mathbf{A}$ is regularized and the unstable least-squares estimate $\mathbf{m}^{est}$ is consequently smoothed to greatly reduce the influence of noise in $\mathbf{d}$, hopefully without distorting the resulting smoothed image too far from the true $\mathbf{m}$ (Titterington, 1985).

The concept of regularization was introduced by Tikhonov in 1963 in order to improve the quality

of the inversion. This theory was studied by many researchers, and we use the approach of Twomey (1963). See Bassrei & Rodi (1993) for more details about names and history in regularization theory. Consider the following objective function:

$$\Phi(\boldsymbol{m}) = \boldsymbol{e}^T\boldsymbol{e} + \lambda(\boldsymbol{D}_l\boldsymbol{m})^T\boldsymbol{D}_l\boldsymbol{m}, \qquad (7)$$

where λ is the regularization parameter and $\mathbf{D}_l$ is the l-order derivative matrix. The estimated model of Equation (7) is given by

$$\boldsymbol{m}^{est} = (\boldsymbol{A}^T\boldsymbol{A} + \lambda\boldsymbol{D}_l^T\boldsymbol{D}_l)^+\boldsymbol{A}^T\boldsymbol{d}^{obs}. \qquad (8)$$

Notice that if $\lambda = 0$ we obtain the standard least squares, and the least squares is said to be damped if $\boldsymbol{D}_0^T\boldsymbol{D}_0 = \boldsymbol{I}$. If $\mathbf{D}$ is the first derivative matrix then the regularization is called to be first order and so on. Each 2-D model was scanned line by line to be represented by a single vector, that is, rasterized. It simplifies the form of the discrete derivative approximation matrix, which resembles a regular pattern. Thus, the matrices $\mathbf{D}_1$ and $\mathbf{D}_2$ may be represented by the following templates:

$$\boldsymbol{D}_1 = \begin{pmatrix} -1 & 1 & 0 & 0 & 0 & 0 & 0 & \cdots & 0 \\ 0 & -1 & 1 & 0 & 0 & 0 & 0 & \cdots & 0 \\ \vdots & & & \vdots & \ddots & \vdots & & & \vdots \\ 0 & \cdots & 0 & 0 & 0 & 0 & -1 & 1 & 0 \\ 0 & \cdots & 0 & 0 & 0 & 0 & 0 & -1 & 1 \end{pmatrix}, \qquad (9)$$

and

$$\boldsymbol{D}_2 = \begin{pmatrix} 1 & -2 & 1 & 0 & 0 & 0 & 0 & \cdots & 0 \\ 0 & 1 & -2 & 1 & 0 & 0 & 0 & \cdots & 0 \\ \vdots & & & \vdots & \ddots & \vdots & & & \vdots \\ 0 & \cdots & 0 & 0 & 0 & 1 & -2 & 1 & 0 \\ 0 & \cdots & 0 & 0 & 0 & 0 & 1 & -2 & 1 \end{pmatrix}. \qquad (10)$$

For the determination of the optimum regularization parameter λ we used the GCV (generalized cross validation) approach. GCV is based on the principle of cross validation, that is, the regularized inverse problem is solved by making M realizations and omitting, at each realization, one point of the observed data. For each realization a specified regularization parameter λ is used. It is expected that the selected λ is adequate, that is, the calculated data obtained by forward modeling for the k-th realization ($\boldsymbol{d}_k^{calc}(\boldsymbol{m}_k^{est})$) is near to the observed data. Thus the optimum regularization parameter is the one which minimizes the conventional cross validation function $V_0(\lambda)$ (Golub et al., 1979; Wahba, 1990) expressed by:

$$V_0(\lambda) = \sum_{k=1}^{N} [\boldsymbol{d}_k^{obs} - \boldsymbol{d}_k^{calc}(\boldsymbol{m}_k^{est})]^2. \qquad (11)$$

The same function can be evaluated in a more efficient way, not demanding the solution of the inverse problem for each omitted data, by using the following expression (Wahba, 1990):

$$V_0(\lambda) = \sum_{i=1}^{N} \frac{[\boldsymbol{d}_i^{obs} - \boldsymbol{d}_i(\boldsymbol{m}_\lambda)]^2}{[1 - B_{ii}(\lambda)]^2}. \qquad (12)$$

where $\boldsymbol{m}_\lambda = (\boldsymbol{A}^T\boldsymbol{A} + \lambda\boldsymbol{D}_l^T\boldsymbol{D}_l)^{-1}\boldsymbol{A}^T\boldsymbol{d}^{obs}$ is the solution of the inverse problem for a particular value of λ, and B_{ii} is the i-th element of the diagonal matrix $\boldsymbol{B} = \boldsymbol{A}(\boldsymbol{A}^T\boldsymbol{A} + \lambda\boldsymbol{D}_l^T\boldsymbol{D}_l)^{-1}\boldsymbol{A}^T$.

Modifying the expression of conventional cross validation function, one obtains the generalized cross validation function or GCV as given by Wahba (1990):

$$V_0(\lambda) = \sum_{i=1}^{N} \frac{\left\|\boldsymbol{d}_i^{obs} - \boldsymbol{d}(\boldsymbol{m}_\lambda)\right\|^2}{\{\mathrm{tr}[\mathbf{I} - \mathbf{B}(\lambda)]\}^2}. \qquad (13)$$

which is invariant under an orthogonal transformation. In the denominator of Equation (13), the trace of a square matrix $\boldsymbol{I} - \boldsymbol{B}(\lambda)$, denoted by $\mathrm{tr}[\mathbf{I} - \mathbf{B}(\lambda)]$, is defined to be the sum of elements on the main diagonal of the matrix.

For the solution of a non-linear problem, one often uses an iterative procedure, where GCV can be applied in each iterative step. In the last iteration, if there is convergence, the changes in model parameters will be small, indicating that the linearized approximations are an adequate description of the non-linear problem. Thus, one can apply GCV both to linear and non-linear problems, that is, since the estimate of optimum regularization parameter in the first iterations is

near the last ones, this approach can be used in non-linear problems. This means that GCV treats in a distinct way the Gaussian noise in observed data in relation to errors generated by the linearized inversion scheme.

Diffraction Tomography Modeling via Born Approximation

In this section, we discuss how to reformulate the original non-linear inversion problem in order to estimate the velocity field using linear inversion, i.e., diffraction tomography. This procedure is performed by considering only first-order scattering and small perturbations on velocity field. From the wave equation:

$$\nabla^2 U(\boldsymbol{r},t) = \frac{1}{c^2(\boldsymbol{r})}\frac{\partial U(\boldsymbol{r},t)}{\partial t^2}, \tag{14}$$

where $U(\boldsymbol{r},t)$ is the displacement or pressure field and $c(\boldsymbol{r})$ is the acoustic velocity of the medium. Let us consider that this field can be represented by a harmonic solution $U(\boldsymbol{r},\omega,t) = e^{-i\omega t}P(\boldsymbol{r},\omega)$. The resulting wave equation in frequency domain is the Helmholtz equation:

$$[\nabla^2 + k^2]P(\boldsymbol{r},\omega) = 0, \tag{15}$$

where $k = k(r,\omega) = \sqrt{k_x^2 + k_y^2}$.

Some assumptions are made in order to further simplify the discussion without loss of generality since its formulation can be extended to a wider class of problems if needed. It is assumed that the medium is 2-D and acoustic, the incident field propagation is limited to a certain area $A(\boldsymbol{r}')$, and that there is a constant background velocity c_0.

Instead of using the velocity field directly, it is mapped into a velocity perturbation called the object function, which is more suitable to achieve the aimed linear formulation. The object function represents the perturbation of the velocity field at each point $\boldsymbol{r}$ in relation to the background velocity and it is defined as:

$$O(\boldsymbol{r}) = 1 - \frac{c_0^2}{c^2(\boldsymbol{r})}. \tag{16}$$

After simple algebraic manipulations, the object function is employed to redefine the wavenumber as its function. Equation (16) can be substituted into the Helmholtz equation, yielding:

$$[\nabla^2 + k_0^2]P_S(\boldsymbol{r}) = k_0^2 O(\boldsymbol{r})[P_O(\boldsymbol{r}) + P_S(\boldsymbol{r})], \tag{17}$$

where k_0 is the homogeneous wavenumber, $P_O(\boldsymbol{r})$ is the incident field and $P_S(\boldsymbol{r})$ is the scattered field.

The obtained differential equation has a well-known integral solution (Lo & Inderwiesen, 1994), which is the Lippmann-Schwinger equation:

$$P_S(\boldsymbol{r}) = -k_0^2 \int_{A(\boldsymbol{r}')} O(\boldsymbol{r}')G(\boldsymbol{r},\boldsymbol{r}')[P_O(\boldsymbol{r}') + P_S(\boldsymbol{r}')]\, d\boldsymbol{r}'. \tag{18}$$

This inverse scattering procedure is performed by estimating the object function from the scattered field, which is done by solving the Lippmann-Schwinger integral equation. Although this equation is non-linear, it can be linearized, for example, via the first order Born approximation, which is valid for weak scattering of the incident field.

The total field $P_T(\boldsymbol{r})$ is the sum of the incident field $P_O(\boldsymbol{r})$ and the scattered field $P_S(\boldsymbol{r})$: $P_T(\boldsymbol{r}) = P_O(\boldsymbol{r}) + P_S(\boldsymbol{r})$. We assume in Equation (18) that the scattered field is much weaker than the incident field ($P_S(\boldsymbol{r}) << P_O(\boldsymbol{r})$), in order to obtain a linear relationship between $O(\boldsymbol{r})$ and $P_S(\boldsymbol{r})$:

$$P_S(\boldsymbol{r}) = -k_0^2 \int_{A(\boldsymbol{r}')} O(\boldsymbol{r}')G(\boldsymbol{r},\boldsymbol{r}')P_O(\boldsymbol{r}')\, d\boldsymbol{r}'. \tag{19}$$

The incident field generated by a line source at $\boldsymbol{r}_S$ (outside$A(\boldsymbol{r}')$ is represented by the Green's function for acoustic propagation (Wu & Toksöz, 1987):

$$P_O(\boldsymbol{r}) = G(\boldsymbol{r}',\boldsymbol{r}_S), \tag{20}$$

which is substituted into the linear relationship between $O(\boldsymbol{r})$ and $P_S(\boldsymbol{r})$. Thus, the scattered field in $A(\boldsymbol{r})$ registered by a receptor in $\boldsymbol{r}_G$ can be rewritten as:

$$P_S(\boldsymbol{r}) = -k_0^2 \int_{A(\boldsymbol{r}')} O(\boldsymbol{r}')G(\boldsymbol{r}_G, \boldsymbol{r}')G(\boldsymbol{r}', \boldsymbol{r}_S)\, d\boldsymbol{r}'. \quad (21)$$

The Equation (21) can be easily discretized (Rocha-Filho et al., 1996), yielding the aimed linear formulation $\boldsymbol{d}^{obs} = \boldsymbol{Am}$, which has to be inverted in order to compute the object function $O(\boldsymbol{r})$. The velocity field is then directly obtained from the object function. The inversion was performed in this work using SVD with regularization, which we described earlier.

NUMERICAL SIMULATIONS

We explore the GCV approach for the selection of the regularization parameter in four synthetic examples for cross hole and VSP geometries. Each model has 225 blocks (15 × 15), that is, the vector of model parameters has 225 components. In all numerical experiments there are 16 sources and 16 receivers, in such a way that the data set has 256 complex numbers. Since we separate the complex numbers in real and imaginary parts, we have in fact 512 data points, making the tomographic matrix overdetermined (512 equations × 225 unknowns). The source emits a monochromatic wave of 200 Hz, and all the simulations were performed with noisy data. Basically, we added Gaussian noise at such a level that the RMS (root mean square) error between the original scattered field and the corrupted field is around 1%. For each example and for each order, we produced three GCV curves. Due to space limitations, we display only some results, although all simulations are summarized in Table 1, where the estimator ε_{rms}^{c} expresses the RMS error of the acoustic velocity:

$$\varepsilon_{rms}^{c} = \frac{\sqrt{\sum_{i=1}^{N}(c_i^{true} - c_i^{est})^2}}{\sqrt{\sum_{i=1}^{N}(c_i^{true})^2}} \times 100\%. \quad (22)$$

In Table 1, besides the results with GCV we also provide the results from L-curve and Θ-curve, taken from Santos & Bassrei (2007).

The scattered field was computed using a second order in time and fourth order in space, finite differences scheme. We adopted a Ricker's wavelet centered around 200 Hz as source, propagating through the medium limited by absorbing boundaries. First, we compute the primary field assuming a homogeneous medium with background velocity. Then we use the object model to compute the total field. We obtain the scattered field by subtracting the primary field from the total field. The Ricker wavelet was deconvolved from the scattered field in order to perform a monochromatic inversion. The calculated field at the source position has some differences of amplitude and phase in relation to the original Ricker's wavelet due to the modeling; these differences were adjusted using an average complex correction factor.

The first synthetic example simulates a diffractor point. The background medium has 4,000 m/s, and the inhomogeneity (diffractor point) is represented by a single block with 4,100 m/s, which means a 2.5% positive anomaly. Figure 1(a) shows the true model. The diffractor point is in fact a 10 m × 10 m square or half wavelength × half wavelength. Figure 1(b) shows the GCV curve for zero order, and its minimum value was used to obtain the estimated model, showed in Figure 1(c). For the second order, the GCV curve, and the reconstructed model are shown in Figures 1(d) and 1(e), respectively. The non-regularized solution, using standard least squares, is showed in Figure 1(f). We notice that the three GCV curves are very similar (the first order is not showed here), and consequently, the results for zero, first, and second orders regularizations are also very similar. This can also be seen by checking Table 1. For this example, the regularized solution was not better than the non-regularized least squares.

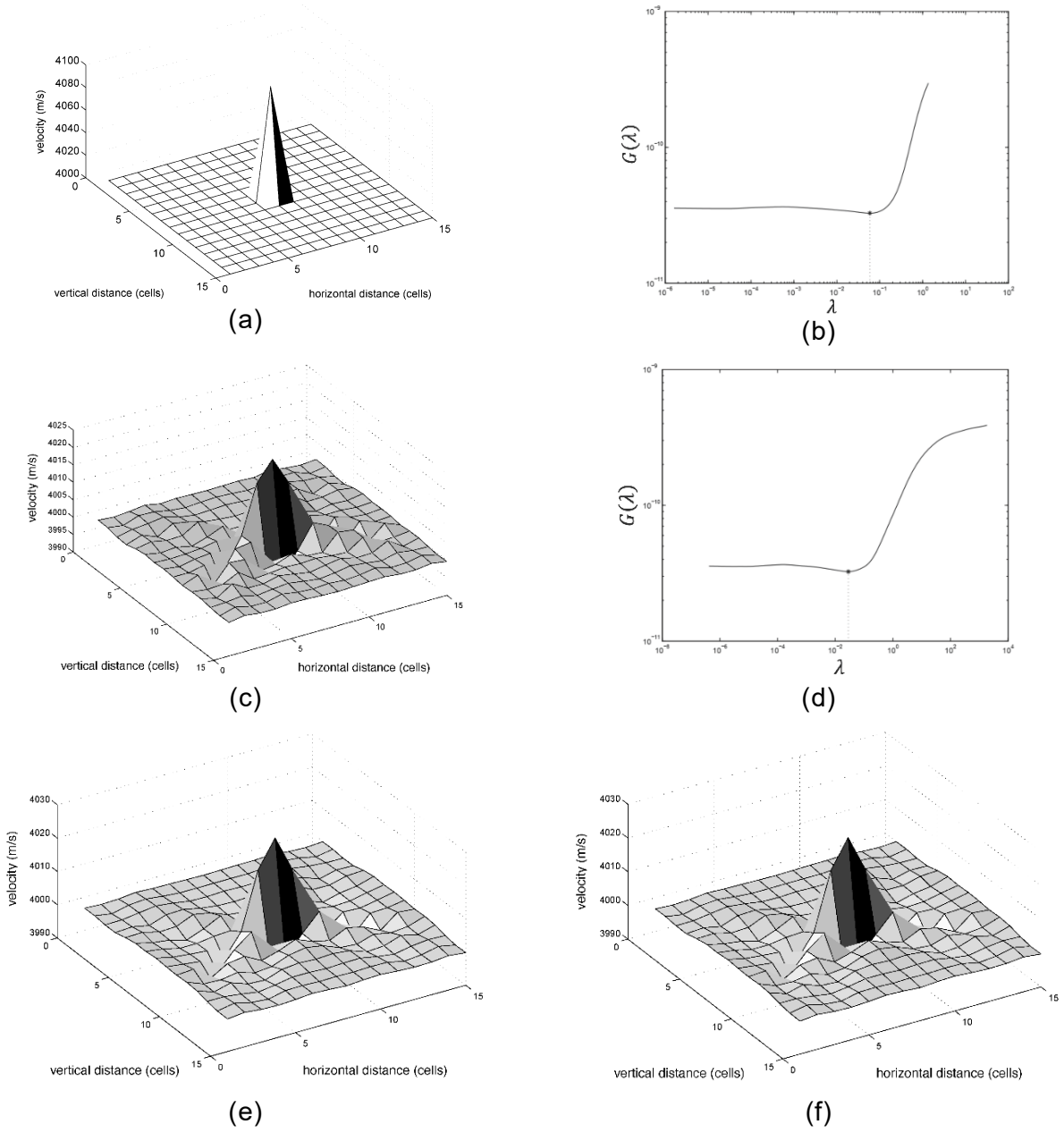

Figure 1 - Diffractor point model. (a) 3-D representation of the true model. (b) GCV curve for zero order. (c) Estimated tomogram for zero order. (d) GCV curve for second order. (e) Estimated tomogram for second order. (f) Estimated tomogram using least squares.

In the second example, there is a homogeneous inclusion in the form of a plus pod within the homogeneous background, which has 3,000 m/s. The inclusion (plus pod) has 3,300 m/s, which represents a positive anomaly of 10%. The plus pod true model can be seen in Figure 2(a). In terms of wavelength, the plus pod has a diameter of 5.3 wavelengths. Figure 2(b) shows the GCV curve for zero order. The minimum value of Figure 2(b) was used to obtain the estimated model showed in Figure 2(c). For the second order, the GCV curve, and the reconstructed model are shown in Figures 2(d) and 2(e), respectively. The least squares solution is presented in Figure 2(f). Comparing Figure 2(f) to Figure 2(c) or to Figure 2(e), we can conclude the necessity of some kind of regularization. The results displayed in Table 1 corroborate this conclusion.

Table 1 - Selection of the best regularization parameter λ^{best} through three different methods and the correspondent value of the estimator ε_{rms}^{c}, computed using Equation (22).

Model	Method	λ^{best}	ε_{rms}^{c}
example 1: diffractor point cross-hole	order 0: L-curve	0.0008	0.07
	order 0: Θ-curve	0.0666	0.06
	order 0: GCV	0.0589	0.06
	order 1: L-curve	0.0006	0.07
	order 1: Θ-curve	0.0769	0.05
	order 1: GCV	0.0435	0.06
	order 2: L-curve	0.0003	0.07
	order 2: Θ-curve	0.0514	0.05
	order 2: GCV	0.0286	0.06
	least squares	---	0.06
example 2: plus pod cross-hole	order 0: L-curve	0.0060	0.69
	order 0: Θ-curve	0.0045	0.78
	order 0: GCV	0.0084	0.60
	order 1: L-curve	0.0111	0.52
	order 1: Θ-curve	0.0061	0.55
	order 1: GCV	0.0058	0.56
	order 2: L-curve	0.0041	0.53
	order 2: Θ-curve	0.0038	0.54
	order 2: GCV	0.0031	0.56
	least squares	---	2.68
example 3: reef cross-hole	order 0: L-curve	0.1234	0.51
	order 0: Θ-curve	0.1322	0.51
	order 0: GCV	0.2100	0.50
	order 1: L-curve	0.1599	0.51
	order 1: Θ-curve	0.3035	0.48
	order 1: GCV	0.5457	0.48
	order 2: L-curve	0.2449	0.53
	order 2: Θ-curve	0.4784	0.49
	order 2: GCV	0.7023	0.48
	least squares	---	0.53
example 4: reef VSP	order 0: L-curve	0.2139	0.60
	order 0: Θ-curve	0.2256	0.60
	order 0: GCV	0.1083	0.63
	order 1: L-curve	0.2783	0.55
	order 1: Θ-curve	0.2971	0.55
	order 1: GCV	0.6596	0.53
	order 2: L-curve	0.8463	0.53
	order 2: Θ-curve	0.5867	0.54
	order 2: GCV	0.7890	0.53
	least squares	---	0.61

The third example, displayed in Figure 3(a), is a simple representation of a reef, as a possible oil reservoir. The acquisition geometry is still cross-hole like the first and the second examples. The background medium has 4,000 m/s. There is also a low velocity layer, with 3,900 m/s, which means a minus 2.5% contrast. The central inhomogeneity (the reef) has 4,100 m/s which is equivalent to a plus 2.5% anomaly. In terms of wavelength the reef is 3.5 wavelengths × 1 wavelength, and the low velocity layer is 7.5 wavelengths × 1 wavelength. Figure 3(b) shows the GCV curve for zero order, from which the minimum value was used to obtain the estimated model showed in Figure 3(c). For the second order, the GCV curve and the reconstructed model are shown in Figures 3(d) and 3(e), respectively. The least squares solution is presented in Figure 3(f). Figure 3(f) displays a reasonable result, but if compared to the regularized solutions, that is, Figure 3(c) or Figure 3(e), it is the worst image, and with the highest value of the ε_{rms}^{c} estimator. The best result, both in terms of quality and error, is provided by the second order GCV regularization.

For the VSP geometry, the true model is showed in Figure 4(a) which is the reef displayed in Figure 3(a). The sources are still located in a hole but the receivers are now located at the surface. Figure 4(b) shows the GCV curve for zero order, and its minimum was used to obtain the estimated model showed in Figure 4(c). For the second order, the GCV curve and the reconstructed model, are shown in Figures 4(d) and 4(e), respectively. The least squares solution is presented in Figure 4(f), which is completely inconsistent. The image obtained with zero order regularization is also very poor, and the first order (not showed) is poor to reasonable, whereas the second order provided the best image. Again, the results displayed in Table 1 corroborate this conclusion.

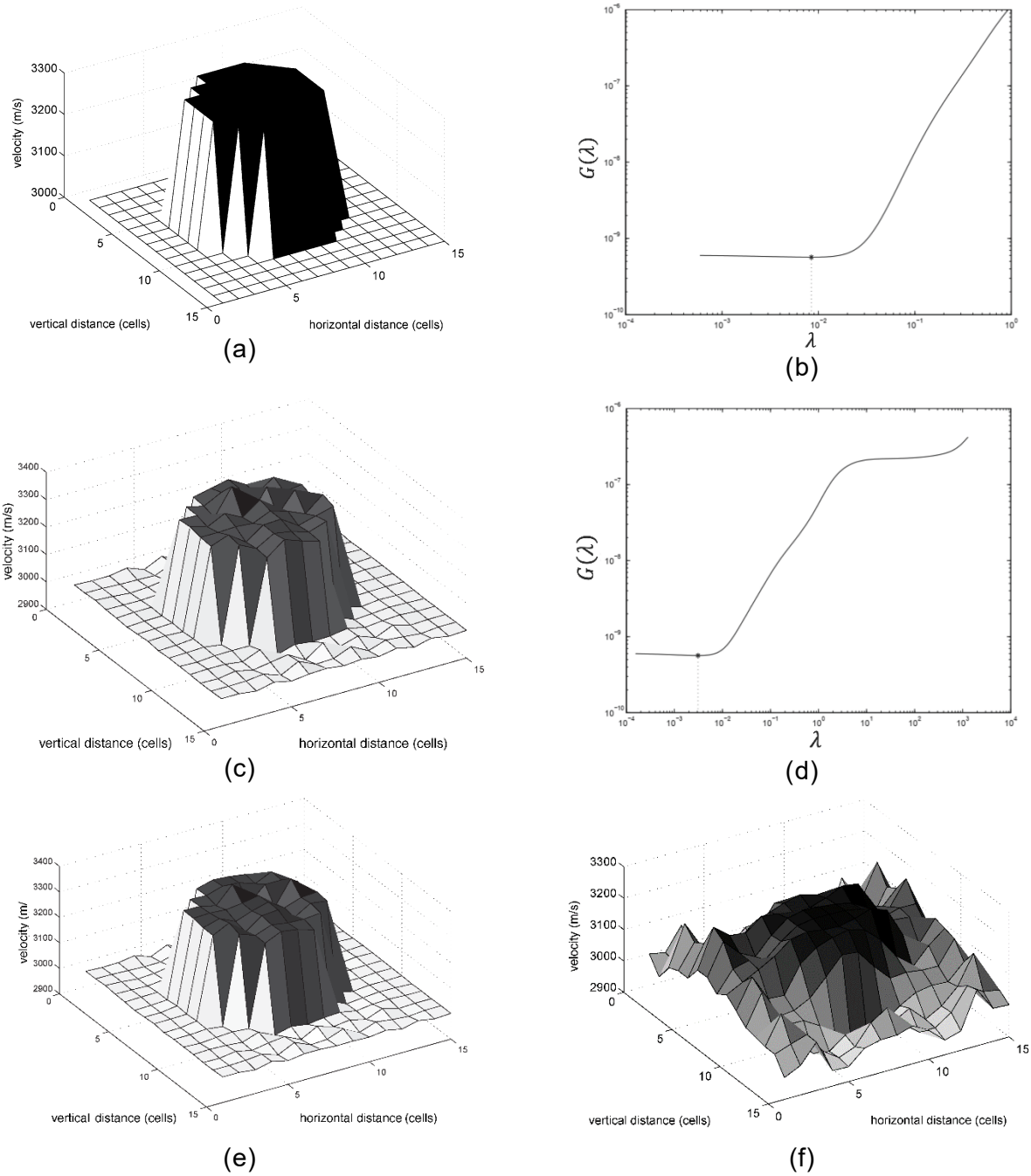

Figure 2 - Plus pod model. (a) 3-D representation of the true model. (b) GCV curve for zero order. (c) Estimated tomogram for zero order. (d) GCV curve for second order. (e) Estimated tomogram for zero order. (f) Estimated tomogram using least squares.

CONCLUSIONS

From four sets of overdetermined synthetic examples corrupted by noise and with an ill-conditioned kernel matrix, we have shown that the regularization algorithm and the use of GCV for the selection of the regularization parameter are feasible in linear geophysical diffraction tomography. The comparison of the results, both visually and quantitatively, with the non-regularized solution confirms that some kind of regularization is necessary. We considered three orders of regularization, which are equivalent to the order of

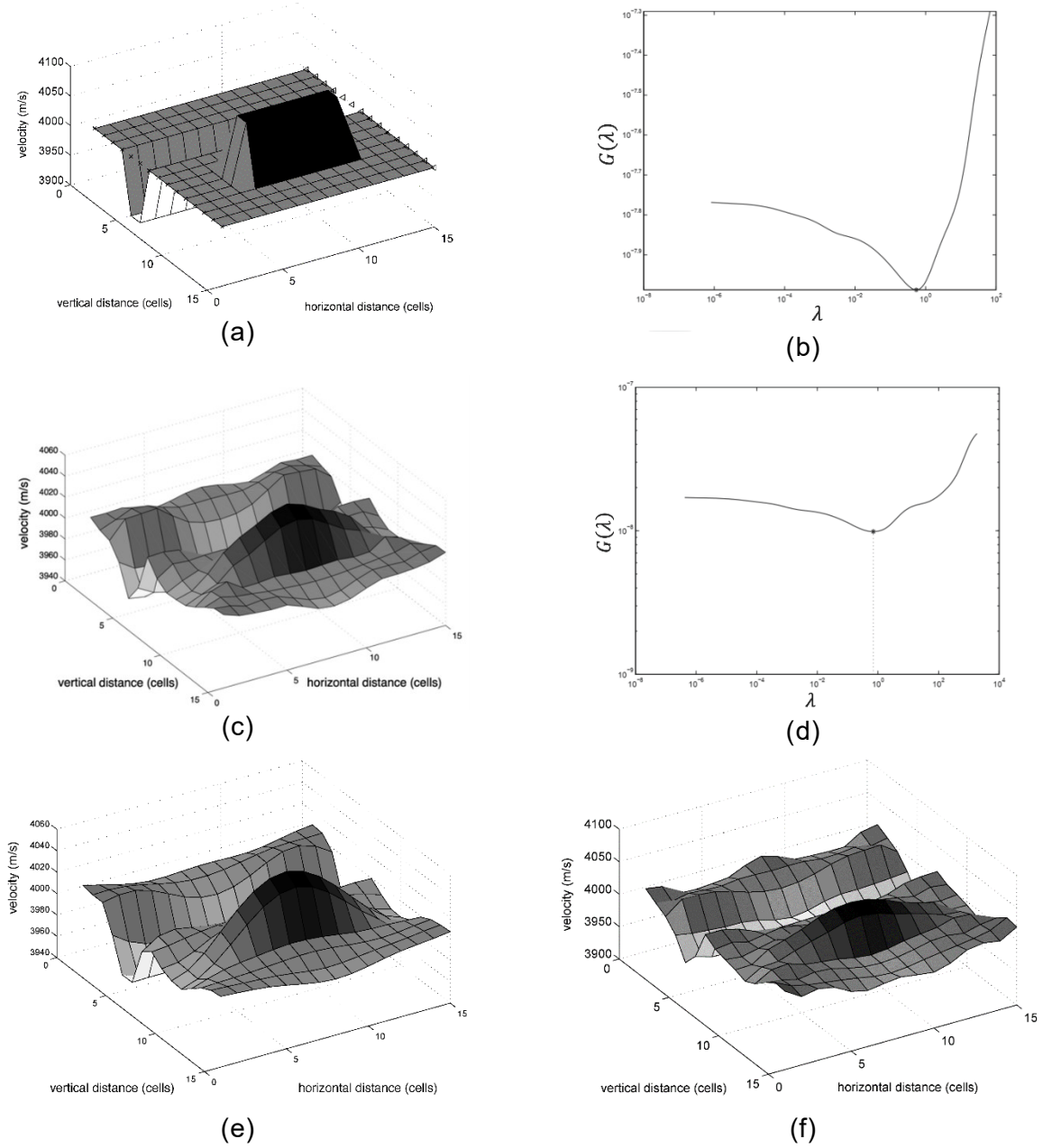

Figure 3 - Simple reef model. Cross-hole geometry data acquisition. (a) 3-D representation of the true model. (b) GCV curve for zero order. (c) Estimated tomogram for zero order. (d) GCV curve for second order. (e) Estimated tomogram for second order. (f) Estimated tomogram using least squares.

the derivative matrix. One important aspect is the selection of the regularization parameter, usually chosen by some trial and error approach. The results with GCV are consistent, providing good approximations to the true model, even considering that Gaussian noise is added to the scattered field. In general, GCV proved to be as efficient as the other two approaches used for comparison, L-curve and Θ-curve, and sometimes more efficient. Also, the visual identification of the optimum regularization parameter is more straightforward in GCV when compared to the other two approaches.

ACKNOWLEDGMENTS

This work was carried out with the support of the Coordenação de Aperfeiçoamento de Pessoal de Nível Superior - Brasil (CAPES) – Financing Code 001. The authors also thank Fundação de Amparo à

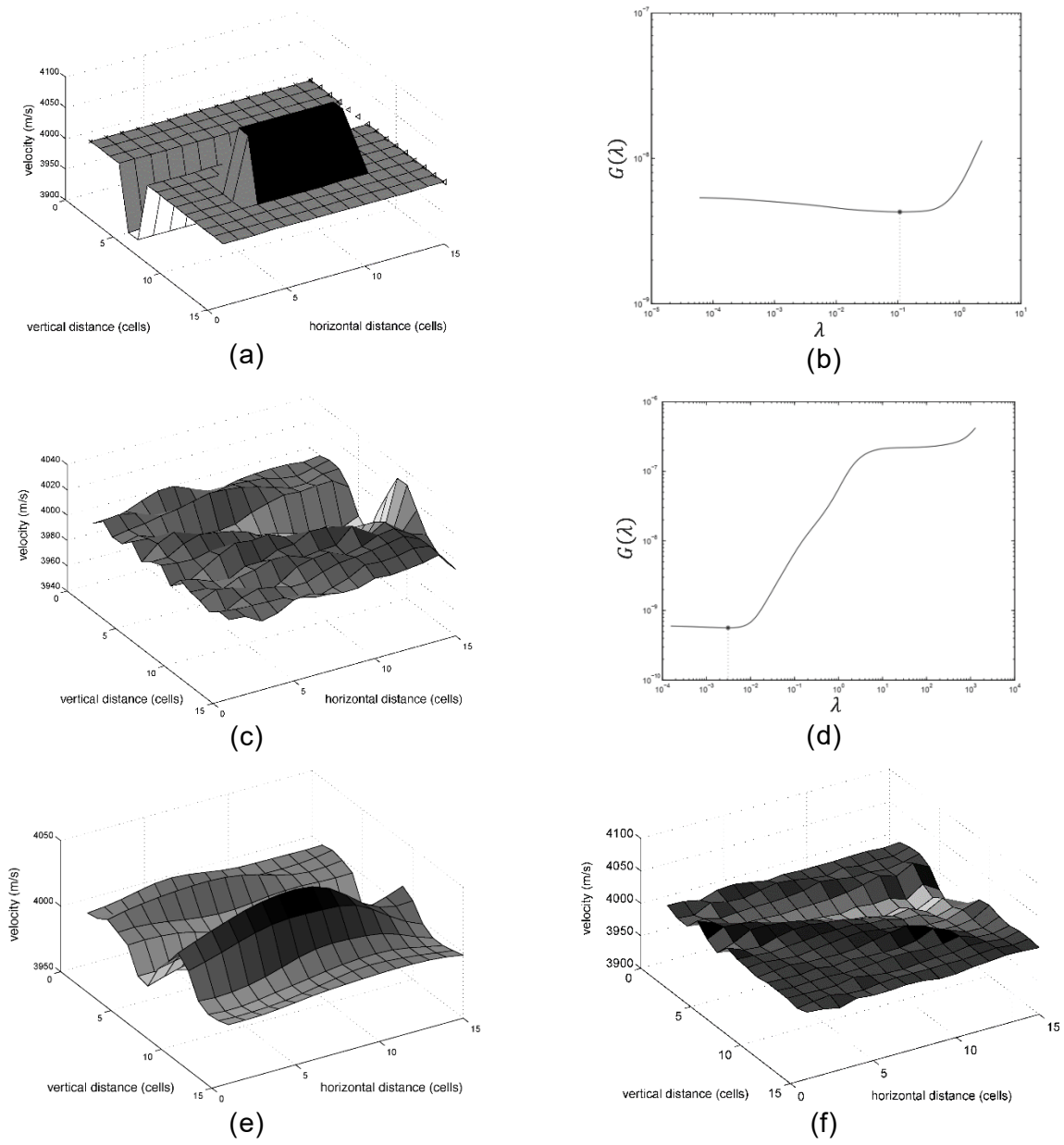

Figure 4 - Simple reef model. VSP geometry data acquisition. (a) 3-D representation of the true model. (b) GCV curve for zero order. (c) Estimated tomogram for zero order. (d) GCV curve for second order. (e) Estimated tomogram for second order. (f) Estimated tomogram using least squares.

Pesquisa do Estado da Bahia (FAPESB) for project PIE00005/2016, Infrastructure Edict 003/2015. A. Bassrei thanks Conselho Nacional de Desenvolvimento Científico e Tecnológico (CNPq) for a research fellowship and for supporting the Instituto Nacional de Ciência e Tecnologia em Geofísica do Petróleo (INCT-GP) project.

REFERENCES

BASSREI A & RODI WL. 1993. Regularization and inversion of linear geophysical data. In: 3rd International Congress of the Brazilian Geophysical Society. Rio de Janeiro, RJ, Brazil: SBGf. vol. 1, pp. 111–116.

DEVANEY AJ. 1984. Geophysical diffraction tomography. IEEE Transactions on Geoscience

and Remote Sensing, 22: 3–13. DOI: 10.1109/TGRS.1984.350573

FARQUHARSON CG & OLDENBURG DW. 2004. A comparison of automatic techniques for estimating the regularization parameter in non-linear inverse problems. Geophysical Journal International, 156: 411–425. DOI: 10.1111/j.1365-246X.2004.02190.x

GIRAUD J, OGARKO V, LINDSAY M, PAKYUZ-CHARRIER E, JESSELL M & MARTIN R. 2019. Sensitivity of constrained joint inversions to geological and petrophysical input data uncertainties with posterior geological analysis. Geophysical Journal International, 218: 666–688. DOI: 10.1093/gji/ggz152

GOLUB G, HEATH M & WAHBA G. 1979. Generalized cross validation as a method for choosing a good ridge parameter. Technometrics, 21: 215–224. DOI: 10.1080/00401706.1979.10489751

GUIZAR-SICAIROS M, GEORGIADIS M & LIEBI M. 2020. Validation study of small-angle X-ray scattering tensor tomography. Journal of Synchrotron Radiation, 27: 779–787. DOI: 10.1107/S1600577520003860

HARRIS JM. 1987. Diffraction tomography with arrays of discrete sources and receivers. IEEE Transactions on Geoscience and Remote Sensing, GE-25: 448–455. DOI: 10.1109/TGRS.1987.289856

LAY-EKUAKILLE A, PARISET C & TROTTA A. 2010 Leak detection of complex pipelines based on the filter diagonalization method: robust technique for eigenvalue assessment. Measurement Science and Technology, 21: 115403 (11 pp). DOI: 10.1088/0957-0233/21/11/115403

LO T-W & INDERWIESEN PL 1994. Fundamentals of Seismic Tomography. Society of Exploration Geophysicists, Tulsa, OK, 187 pp. DOI: 10.1190/1.9781560802334

MENKE W. 2012. Geophysical Data Analysis: Discrete Inverse Theory. 3rd ed., Academic Press, San Diego, US. 330 pp.

MOJICA OF & BASSREI A. 2015. Regularization parameter selection in the 3-D gravity inversion of the basement relief using GCV: A parallel approach. Computers & Geosciences, 82: 205–213. DOI: 10.1016/j.cageo.2015.06.013

NIKNAM SHAHRAK M, SHAHSAVAND A & OKHOVAT A. 2013. Robust PSD determination of micro and meso-pore adsorbents via novel modified U curve method. Chemical Engineering Research and Design, 91: 51–62. DOI: 10.1016/j.cherd.2012.07.003

OLIVEIRA NP & BASSREI A. 2015. Tomografia eletromagnética de tempos de trânsito: aplicação do GCV para a busca do parâmetro de regularização. Sitientibus Série Ciências Físicas, 11: 1–10. DOI: 10.13102/sscf.v11i0.5261

REITER TD & RODI W. 1996. Nonlinear waveform tomography applied to crosshole seismic data. Geophysics, 61: 902–913. DOI: 10.1190/1.1444015

ROCHA-FILHO AA, HARRIS JM & BASSREI A. 1996. A simple matrix formulation diffraction tomography algorithm. In: 39th Brazilian Congress of Geology. Salvador, BA, Brazil: SBG. vol. 2, p. 312–315.

ROCHA-FILHO AA, HARRIS JM & BASSREI A. 1997. Integrated inversion of seismic data using diffraction tomography [in Portuguese]. In: 5th International Congress of the Brazilian Geophysical Society. São Paulo, SP, Brazil: SBGf. vol. 2, p. 630–634.

RODRIGUES VHSR & BASSREI A. 2016. Seismic traveltime tomography applied to data from Miranga Field, Recôncavo Basin, Brazil. Brazilian Journal of Geophysics, 34: 351–362. DOI: 10.22564/rbgf.v34i3.856

SANDE D, BASSREI A & HARRIS J. 2019. New iterative and multi-frequency approaches in geophysical diffraction tomography. Brazilian Journal of Geophysics, 37: 187–197. DOI: 10.22564/rbgf.v37i2.2000

SANTOS ETF & BASSREI A. 2007. L- and Θ-curve approaches for the selection of regularization parameter in geophysical diffraction tomography. Computers & Geosciences, 33: 618–629. DOI: 10.1016/j.cageo.2006.08.013

SILVA CJMG & BASSREI A. 2016. Singular value selection and generalized cross validation in multi-frequency seismic diffraction tomography for CO_2 injection monitoring. Brazilian Journal of Geophysics, 34: 175–192. DOI: 10.22564/rbgf.v34i2.791

SLANEY M, KAK AC & LARSEN LE. 1984. Limitations of Imaging with First-order diffraction

Tomography. IEEE Transactions on Microwave Theory and Techniques, 32: 860–874. DOI: 10.1109/TMTT.1984.1132783

THOMPSON DR, RODI W & TOKSÖZ MN. 1994. Nonlinear seismic diffraction tomography using minimum structure constraints. Journal of the Acoustical Society of America, 95: 324–330. DOI: 10.1121/1.408365

TITTERINGTON DM. 1985. General structure of regularization procedures in image reconstruction. Astronomy and Astrophysics, 144: 381–387.

TWOMEY S. 1963. On the numerical solution of Fredholm integral equations of the first kind by the inversion of the linear system produced by quadrature. Journal of the Association of Computing Machines, 10: 97–101. DOI: 10.1145/321150.321157

WAHBA G. 1990 Splines models for observational data. CBMS-NSF Regional Conference Series in Applied Mathematics. SIAM - Society for Industrial and Applied Mathematics, Philadelphia. 161 pp. DOI: 10.1137/1.9781611970128

WU R.-S & TOKSÖZ MN. 1987. Diffraction tomography and multisource holography applied to seismic imaging. Geophysics, 52: 11–25. DOI: 10.1190/1.1442237

YAO ZS & ROBERTS RG. 1999. A practical regularization for seismic tomography. Geophysical Journal International, 138: 293–299. DOI: 10.1046/j.1365-246X.1999.00849.x

ZHANG Y. 2011. Novel Method for Selection of Regularization Parameter in the Near-field Acoustic Holography. Chinese Journal of Mechanical Engineering, 24: 285. DOI: 10.3901/CJME.2011.02.285

E.T.F.S.: developed this study, processed the data, generated the figures, interpreted the results and wrote the first version of the manuscript. **A.B.:** supervised the research, contributed to the results discussion, and reviewed the manuscript. **J.M.H.:** co-supervised the research, contributed to the results discussion and reviewed the manuscript.

Received on October 31, 2020 / Accepted on January 11, 2021
Recebido em 31 de outubro de 2020 / Aceito em 11 de janeiro de 2021